Journal of Catalysis 263 (2009) 98–103

Contents lists available at ScienceDirect

Journal of Catalysis

www.elsevier.com/locate/jcat

Scanning tunneling microscopy studies of TiO_2-supported hydrotreating catalysts: Anisotropic particle shapes by edge-specific MoS_2–support bonding

Jakob Kibsgaard [a], Bjerne S. Clausen [b], Henrik Topsøe [b], Erik Lægsgaard [a], Jeppe V. Lauritsen [a,*], Flemming Besenbacher [a]

[a] Interdisciplinary Nanoscience Center (iNANO) and Department of Physics and Astronomy, Aarhus University, DK-8000 Aarhus C, Denmark
[b] Haldor Topsøe A/S, Nymøllevej 55, DK-2800 Lyngby, Denmark

ARTICLE INFO

Article history:
Received 11 November 2008
Revised 27 January 2009
Accepted 27 January 2009
Available online 14 February 2009

Keywords:
Hydrotreating
Hydrodesulfurization
HDS
Model catalyst
Scanning tunneling microscopy
STM
Molybdenum disulfide
MoS_2 nanoclusters
Morphology
Support effect
Titania
TiO_2

ABSTRACT

By means of scanning tunneling microscopy (STM) studies of MoS_2 nanoparticles on a rutile $TiO_2(110)$ support, we have studied fundamental atomic-scale aspects of the particle–support interactions for metal-sulfide hydrotreating catalysts on a metal oxide support. The STM results reveal that strong particle–support interactions at the particle edges have an overriding effect on the equilibrium shape of single-layer MoS_2 nanoparticles on the TiO_2 support. The single-layer MoS_2 nanoparticles are observed to be in flat contact with the metal oxide surface and preferentially adopt the shape of uniform elongated platelets oriented along one of the high-symmetry directions of the two-fold symmetric TiO_2 substrate. Depending on the specific orientation relative to the substrate, the MoS_2 particles exhibit two distinct widths of 33 or 38 Å which originate from the optimized lattice matching distances of the MoS_2 lattice along either of the high symmetry directions of the $TiO_2(110)$ support. Atom-resolved STM images furthermore reveal that the (0001) basal plane of MoS_2 appears unperturbed showing that predominantly strong edge bonding effects control the particle morphology in this catalyst. The experimental STM results thus give strong support to recent edge-bonding models from the literature investigating the adhesion of MoS_2 nanoparticles to metal oxides by chemical linkages at the particle edges.

1. Introduction

Hydrotreating of fossil fuels covers a broad range of catalytic processes applied to upgrade the crude oil and to remove environmental harmful compounds such as sulfur [1,2]. Stricter environmental legislation has generated a large demand for ultra-low sulfur transportation fuels and consequently increased attention has been directed toward obtaining a detailed fundamental understanding of the hydrodesulfurization (HDS) catalyst [3–6]. The most widely used hydrotreating catalyst consists of metal oxide supported molybdenum disulfide (MoS_2) or alternatively tungsten disulfide (WS_2) single-layer nanoparticles, typically promoted by a small amount of either Co or Ni [1,7]. Due to the highly dispersed nature of the catalyst and a weak contrast of the sulfide phase in, e.g. electron microscopy, it has been difficult to study even basic aspects of the morphology of the active single-layer MoS_2 nanoparticles in real catalysts [1,8–10] and consequently a number of very fundamental properties related to the catalytic function of the nanoparticles remain disputed.

Recently it has, however, been shown how scanning tunneling microscopy (STM) can be used to image directly the atomic-scale structure of MoS_2 nanoparticles synthesized on an inert gold substrate as a model system for the HDS catalyst. This approach has allowed us for the first time to get valuable information on a number of fundamental properties related to the particle shape [11–13], the edge structure [12], the location and nature of the active sites [11,14], and the role of Co and Ni as promoters in the so-called CoMoS and NiMoS promoted hydrotreating catalysts [15,16]. While most of these observations were aimed at studying important intrinsic properties of the active MoS_2 or CoMoS/NiMoS phases only little work has been done on elucidating the influence of other parameters such as the support employed in real catalysts. Recent STM studies of MoS_2 synthesized on graphite gave evidence of a rather weak particle–support interaction [13]. Metal oxides, and in particular alumina in the gamma-form (γ-Al_2O_3), are, however, traditionally the preferred support materials for the active MoS_2 phase. Metal oxides often have an easy obtainable porous structure and the strong bonding properties of the metal oxides favor the synthesis of small MoS_2 particles with a high edge dispersion

* Corresponding author.
E-mail addresses: jvang@inano.dk (J.V. Lauritsen), fbe@inano.dk (F. Besenbacher).

0021-9517/$ – see front matter
doi:10.1016/j.jcat.2009.01.016

and a high reactivity. In recent years, much work has been aimed at elucidating fundamental relations between catalytic activity and selectivity of the MoS_2 phase and the composition and structure of the support [17–23]. Most notably, this kind of work has led to the classification of "Type I" or "Type II" catalysts characterized by the strength of the particle–support interaction. It was shown that Type II CoMoS nanoparticles have a rather weak support interaction and are much more active than Type I CoMoS particles which interact strongly with the support. The lower activity of the Type I structures was attributed to the formation of chemical linkages (Mo–O–Al) to the support, which modifies the coordination and bonding of the reactive edge sites [21]. Previous FTIR work [17] has also provided solid evidence that such linkages form during calcination of the catalyst precursors for oxide supports, but the exact distribution, the impact on cluster morphology and nature of such linkages in an MoS_2 nanoparticle is still unknown and the influence on the catalytic properties is unclear.

Interestingly, catalysts based on other metal oxide supports, such as zirconia (ZrO_2) or anatase titania (TiO_2), have on the demonstration scale displayed a promisingly high HDS reactivity of thiophene [6,18,19,24], suggesting that also the nature of the chemical linkage (Mo–O–X) is important. Thus, a detailed optimization of the particle–support interaction based on fundamental insight may contribute to the development of better catalysts. Here we investigate by means of STM the structure and morphology of MoS_2 nanoparticles supported on a rutile $TiO_2(110)$ substrate as a convenient model system to experimentally investigate particle–support effects for metal sulfide nanoparticles on a metal oxide.

2. Experimental

The experiments were performed in an ultrahigh-vacuum (UHV) chamber with a base pressure below 1×10^{-10} mbar. The chamber is equipped with standard equipment for surface preparation and analysis using Auger Electron Spectroscopy (AES) and a home-built high-resolution STM [25].

A single crystal rutile $TiO_2(110)$ sample (MTI Corp, USA) was used as a model support in these studies. The surface of the fresh crystal was cleaned using a number of cycles consisting of 20 min of Ar^+ sputtering (1 keV) at room temperature followed by annealing at 900 K for 20 min to restore a flat surface until no contaminants were observed with AES and the STM images revealed a flat and clean surface. At this stage, the titania crystal had obtained a dark blue color, indicating hat the sample was O-deficient, bulk reduced, and conductive.

The MoS_2 nanoparticles were synthesized by evaporating metallic molybdenum (99.9% nominal purity) onto the $TiO_2(110)$ substrate using an e-beam evaporator (Oxford Applied Research, EGCO-4) followed by a high-temperature sulfidation step. The Mo deposition was carried out at 400 K in an H_2S atmosphere corresponding to $\sim 5 \times 10^{-6}$ mbar and subsequently the sample was annealed to 900–950 K for 15 min while keeping the sulfiding atmosphere. For all experiments we deposited a fixed amount of Mo corresponding to ~10% of a monolayer.

3. Results and discussion

3.1. Atomic structure of the rutile $TiO_2(110)$ support

A key finding of this paper is related to the ability of the metal oxide support to steer the shape of the supported MoS_2 nanocluster as determined by the epitaxial relations. We therefore first discuss the atomic structure of the rutile $TiO_2(110)$ surface, which has been extensively studied in the literature as a "prototypical" system for fundamental surface science studies of transition metal oxides [26–28]. As illustrated in the ball model in Fig. 1b, the stoichiometric $TiO_2(110)$ surface consists of alternating rows of fivefold coordinated titanium atoms (grey), Ti(5f), and twofold coordinated (bridging) oxygen atoms (red), O(2f), which protrude about 0.1 Å from the surface. The row structure of the $TiO_2(110)$ surface is revealed in atom-resolved STM images in Fig. 1a. However, constant current STM images in general represent a convolution of the geometric and the electronic structures of the surface [29], and it has been established that STM images of the $TiO_2(110)$ surface are strongly dominated by the electronic structure instead of the actual geometry, so that the Ti troughs counter-intuitively are imaged as the bright rows, whereas the geometric protruding bridging O rows are imaged as dark rows [26]. The bright protrusions located on the dark rows in Fig. 1a have previously been characterized in great detail with STM, and the height, distribution and dynamic behavior of the bright protrusions seen in this study allows us to assign them as bridging hydroxyl groups [30]. The bridging hydroxyl groups appear as a result of dissociation of water from the rest gas in surface oxygen vacancies on a rather short time scale even under UHV conditions, but upon heating above 520 K the hydroxyls are removed from the surface and we can therefore assume that the titania substrate is free of hydroxyls during high temperature synthesis [31–33].

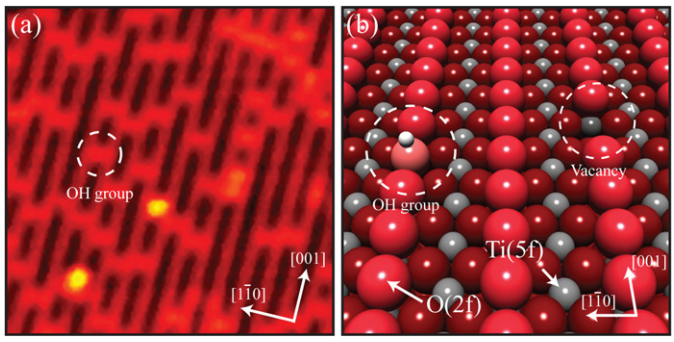

Fig. 1. (a) STM image of the $TiO_2(110)$ surface (100 Å × 100 Å, $I_t = 0.490$ nA and $V_t = 1250$ mV). The predominant bright protrusions on the dark rows are ascribed to bridging hydroxyl groups formed by dissociation of water from the rest gas in oxygen vacancies that are created during the cleaning process. (b) Ball model of the $TiO_2(110)$ surface showing a bridging hydroxyl group and an oxygen vacancy. Color code—Ti gray and O red. (For interpretation of the references to color in this figure legend, the reader is referred to the web version of this article.)

During the sulfidation step in the synthesis we exposed the TiO_2 surface to up to 10^4 L (1 L (Langmuir) = 1×10^{-6} Torr s) of H_2S, which could induce changes in the surface state and structure, either by adsorption or adsorption induced reconstruction. However, in a reference experiment without the Mo deposition, we only find trace amounts of sulfur on the surface with Auger electron spectroscopy (AES) after exposing the annealed $TiO_2(110)$ surface to H_2S. Furthermore, subsequent STM images of the $TiO_2(110)$ surface exposed to H_2S (with and without Mo) always reveal the well-known alternating parallel bright and dark row appearance of the $TiO_2(110)$ surface. We therefore conclude that the MoS_2 nanoparticles are supported on an oxygen terminated $TiO_2(110)$ surface as shown in Fig. 1b exhibiting a low concentration of bridging hydroxyl groups.

3.2. Morphology of the MoS_2 nanoparticles

The temperature of the sulfidation step in the synthesis is observed to have a large impact on the morphology of the synthesized MoS_2 nanoparticles, since those synthesized at 950 K (Fig. 2b, 1000 Å × 1000 Å) are generally found to be much larger and have a pronounced elongated shape compared to MoS_2 nanoparticles synthesized only 50 K lower at 900 K (Fig. 2a,

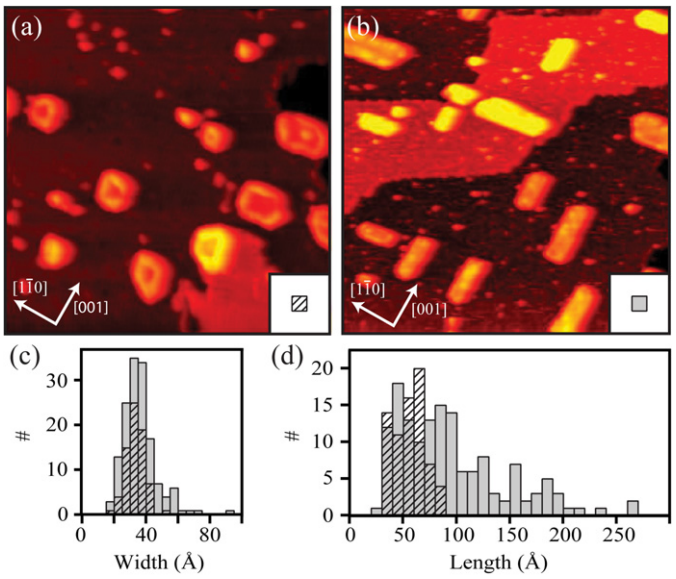

Fig. 2. (a, b) STM images showing the synthesized MoS_2 nanoparticles on a TiO_2 (110) surface. (a) is synthesized at 900 K (500 Å × 500 Å, $I_t = 0.320$ nA, $V_t = 1250$ mV) and (b) is synthesized at 950 K (1000 Å × 1000 Å, $I_t = 0.300$ nA, $V_t = 1250$ mV). (c) Width and (d) length distribution of the MoS_2 nanoparticles, respectively.

500 Å × 500 Å). At both synthesis temperatures, however, we find that the MoS_2 nanoparticles adopt a distinct uniform width, and we explain the observations by a higher mobility of the MoS_2 surface species at 950 K which allows the cluster to fully develop the shape of elongated platelets. The uniform width and the growth mode by elongation are analyzed in detail in the width and length distribution histograms depicted in Figs. 2c and 2d. The STM image in Fig. 3d shows how the particles are capped by 60° bends, and the exact shape of the particle is therefore best described by a hexagon in which two of the parallel sides have been elongated (see ball model in Fig. 4).

Atom-resolved STM images of the MoS_2 particles synthesized at both 900 and 950 K (see, e.g. Fig. 3c) reveal a perfectly crystalline basal plane consisting of hexagonally arranged protrusions with an average interatomic spacing of 3.15 Å. This distance agrees well with the interatomic spacing of the (0001) basal plane of bulk MoS_2, and we thus conclude that the MoS_2 nanoparticles are aligned with the MoS_2(0001) facet in *parallel* with the TiO_2(110) support (i.e. MoS_2 lying completely flat on TiO_2). Due to the semiconducting properties of MoS_2, the apparent height in STM images of the MoS_2 basal plane is observed to be slightly dependent on the applied bias voltage. Only at relatively high tunneling voltages (>1000 mV) does the height of the hexagonal basal plane of the MoS_2 nanoparticles reach an asymptotical value of 4.7 ± 0.5 Å relative to the TiO_2(110) surface matching the expected dimension of a single S–Mo–S layer (core-to-core distance $d_{S-Mo-S} = 3.15$ Å), and we thus conclude that *single-layer* MoS_2 nanoparticles are formed on the TiO_2 surface. At lower bias voltages (<1000 mV) electronic effects become more pronounced since the STM primarily tunnels to electronic states inside the band gap of MoS_2. At the lowest voltages, the characteristic row structure of the TiO_2(110) surface becomes increasingly more visible in STM images on the basal plane of the MoS_2 nanoparticles, as shown in Figs. 3b and 3c. Since this modification is seen only at low bias voltages, we attribute the perturbation to charge transfer to the MoS_2 particle from the bright Ti rows of the TiO_2 substrate, and not from a periodic geometric distortion of the MoS_2 layer from the buckled TiO_2 surface. The relatively unperturbed appearance of the basal plane thus indicates that direct bonding of the interior MoS_2 basal is not present. We also note that another even more pronounced electronic perturbation is revealed by the appearance of the much brighter edges of the particles in the STM images. The bright edges arise due to the presence of metallic

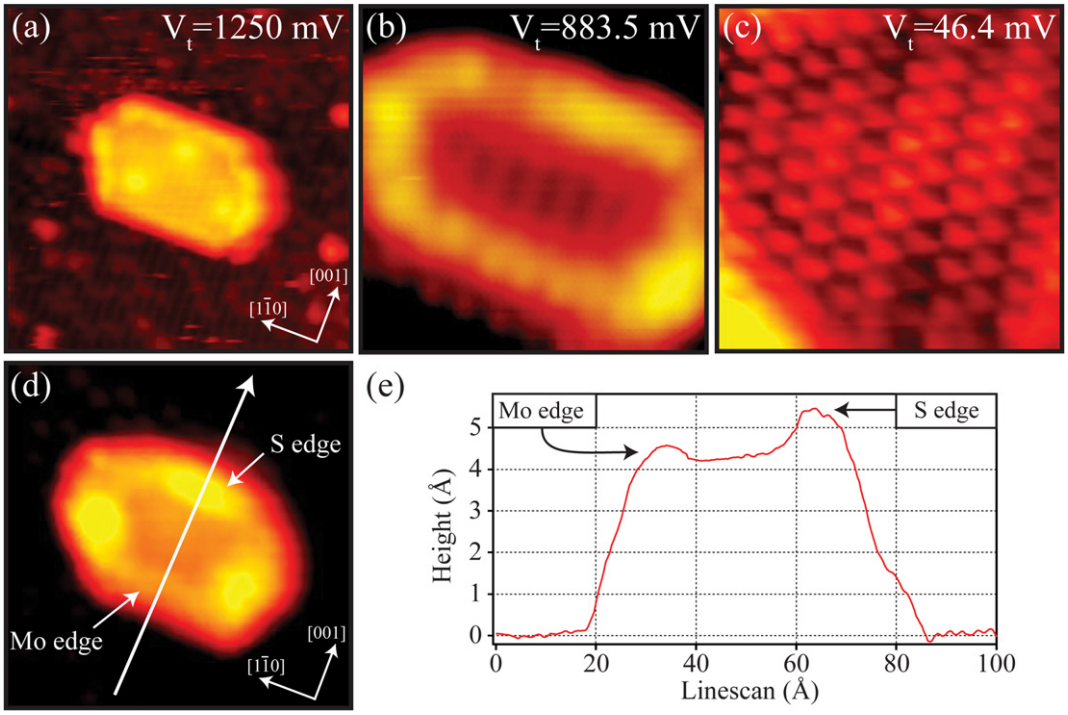

Fig. 3. (a)–(c) STM images showing the bias dependent imaging of the MoS_2 nanoparticles: (a) 200 Å × 200 Å, $I_t = 0.320$ nA, $V_t = 1250$ mV; (b) 70 Å × 70 Å, $I_t = 0.260$ nA, $V_t = 883.5$ mV; and (c) 30 Å × 30 Å, $I_t = 0.390$ nA, $V_t = 46.4$ mV. (d) STM image (100 Å × 100 Å, $I_t = 0.350$ nA, $V_t = 1250$ mV) clearly showing that the MoS_2 nanoparticles expose two different edge terminations: the Mo and S edge, respectively. (e) Line scan across the nanoparticle depicted in (d) as indicated by the white arrow.

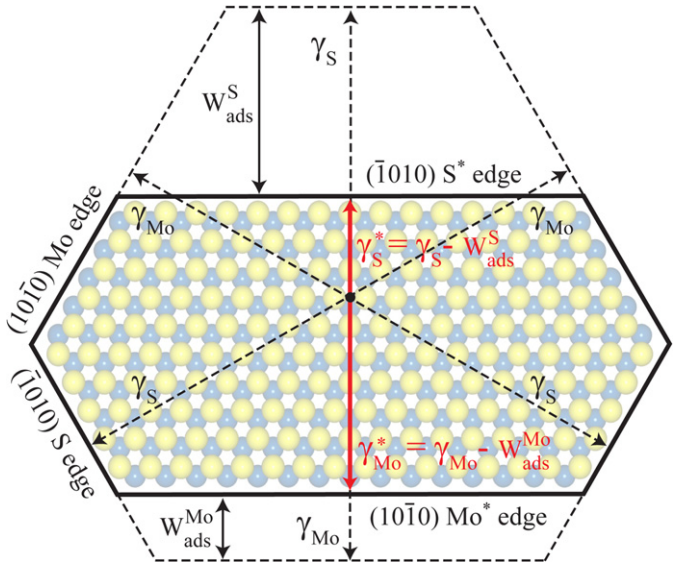

Fig. 4. Schematic Wulff–Kaischew representation of an elongated TiO_2 supported single-layer MoS_2 particle. γ_{Mo} and γ_S denote the edge free energies of the $(10\bar{1}0)$ Mo and the $(\bar{1}010)$ S edges, respectively. The two longer edges of the particle have edge free energies (γ^*_{Mo} and γ^*_S) modified by the work of adhesion (W_{adh}). Color code—Mo blue and S yellow. (For interpretation of the references to color in this figure legend, the reader is referred to the web version of this article.)

one-dimensional edge states of MoS_2 layers [34,35], which have been shown to have catalytic importance and will be discussed later on.

The occurrence of elongated flat-lying MoS_2 particles on TiO_2 in Fig. 2b is interesting and points to a significant anisotropic particle–support interaction at the cluster edges. Previous STM results for MoS_2 nanoparticles synthesized on weakly interacting supports under similar conditions [11,13], have revealed that the equilibrium shape of MoS_2 nanoparticles are rotationally 3-fold symmetric around the (0001) axis (triangular and regular hexagonally truncated shapes) as expected for a "free" particle with a hexagonal lattice structure. These simple shapes can be described in terms of a Wulff construction in which the relative edge free energies of the $(10\bar{1}0)$ S edges and $(\bar{1}010)$ Mo-edges, which terminate the particle, describe the equilibrium shape [36,37]. The elongated single-layer MoS_2 particles capped by 60° bends must for symmetry reasons of the MoS_2 lattice still reflect a particle terminated by three $(\bar{1}010)$-type Mo edges and three $(10\bar{1}0)$-type S edges like a regular MoS_2 truncated triangle (Fig. 4). The different edge lengths, however, imply that edge free energies are perturbed by the substrate in an anisotropic way. The observed shape can in general be represented in the so-called Wulff–Kaischew (WK) construction [38] which extends the Wulff model of free particles and describes the shape of supported nanoparticles by including a contribution of the work of adhesion (W_{adh}) to the edge free energy on the edge which bonds to the substrate [39]. Within this framework, the elongated equilibrium shape of the MoS_2 particles is compatible with a corner truncated triangle [12], which has become further truncated on the two opposite longer edges due to substrate bonding (Fig. 4). Formally, this is explained by a lowering of the edge free energies of one S edge and one Mo edge (γ^*_{Mo} and γ^*_S) compared with the edge free energies of the remaining four shorter edges (γ_{Mo} and γ_S) due to the energy gained by adhesion (W_{adh}) of the particle on these edges. In the present case, we propose that the apparent anisotropic gain in edge free energies (γ^*_{Mo} and γ^*_S) driving the formation of the elongated particle shapes is associated with the favorable formation of "linkages" between the longer edges and the substrate only when a favorable epitaxial relation is present between the MoS_2 lattice and the TiO_2 support.

Large-scale STM images like Fig. 2b indeed reveal that the nanoparticles exclusively orient in two very distinct ways on the $TiO_2(110)$ surface: parallel or perpendicular to the [001] direction. In Fig. 5a is depicted a more detailed analysis of the rotation of the MoS_2 nanoparticles relative to the [001] direction of the $TiO_2(110)$ surface, and it is clearly observed that all of the MoS_2 nanoparticles are oriented either parallel (0°) or perpendicular (90°) to the [001] direction. The clear preference for these two specific orientations of the MoS_2 nanoparticles must be governed by the interfacial bonding between the MoS_2 nanoparticles and the $TiO_2(110)$ support. The three-fold symmetric hexagonal lattice structure of MoS_2 implies that a 60° rotation of an MoS_2 nanoparticle does not change the orientation of the MoS_2 lattice with respect to the two-fold symmetry of the $TiO_2(110)$ surface. However, the fact that no MoS_2 nanoparticles are oriented at an angle of 30° or 60° relative to the [001] direction of the $TiO_2(110)$ surface shows that the interaction between the basal plane of the MoS_2 nanoparticles and the $TiO_2(110)$ support is weak like between layers in bulk MoS_2 and it does not play a role in the bonding of the nanoparticles with respect to the support.

The epitaxial origin of the two distinct orientations of the MoS_2 nanoparticles and the very narrow width distribution is revealed in detail by an analysis of the lattice mismatch between the $MoS_2(0001)$ lattice and the two anisotropic low-index directions of $TiO_2(110)$. Figs. 5c and 5d display the specific width distribution for MoS_2 nanoparticles oriented parallel and perpendicular to the [001] direction of the $TiO_2(110)$ surface, respectively. The nanoparticles oriented parallel to the [001] direction have an average width of 38 ± 1 Å, which is slightly larger than the average width of 33 ± 1 Å for the nanoparticles oriented perpendicular to the [001] direction.

Fig. 5b shows two model slabs of MoS_2 on a $TiO_2(110)$ surface where the bridging oxygen atoms of the substrate are represented by the grid. One slab is oriented parallel and the other perpendicular to the [001] direction, respectively. The bright brim structure (discussed in more detail in the following section) extending along the edge of the MoS_2 nanoparticles (see, e.g. Fig. 2a) can be used to determine the position of the two slabs relative to the surface. Fig. 5e shows an atom-resolved STM image of the edge of an MoS_2 particle oriented parallel to the [001] direction of the $TiO_2(110)$ surface and from the superimposed grid representing the position of the bridging oxygen atoms it is observed that the brim structure is on top of two bridging oxygen rows running in the [001] direction. Accordingly, the model slab oriented parallel to the [001] direction in Fig. 5b has been placed with the brim structure (yellow balls) on top of two bridging rows in the [001] direction. Fig. 5b reveals that in order for both edges parallel to the [001] direction to have this particular strong bonding position on the $TiO_2(110)$ surface, the nanoparticles must have a width of 38.3 Å. In a similar way, Fig. 5f shows the position relative to the $TiO_2(110)$ surface for a nanoparticle oriented perpendicular to the [001] direction, and Fig. 5b shows that these nanoparticles must have a width of 32.8 Å to obtain this particular strong bonding position under both edges parallel to the $[1\bar{1}0]$ direction. Both these widths are in excellent agreement with the experimentally observed widths of the MoS_2 nanoparticles thus providing evidence that epitaxial relations strongly determine both the size and orientation of the MoS_2 particles on $TiO_2(110)$.

The length distribution depicted in Fig. 2d implies the formation of elongated MoS_2 particles with widely different aspect ratios, which in terms of the WK construction implies a variable effective edge free energy (γ^*_{Mo} and γ^*_S) and, hence, adhesion energy on the longer edges (Fig. 4). However, the WK construction only describes the shape of a strain free island on a substrate,

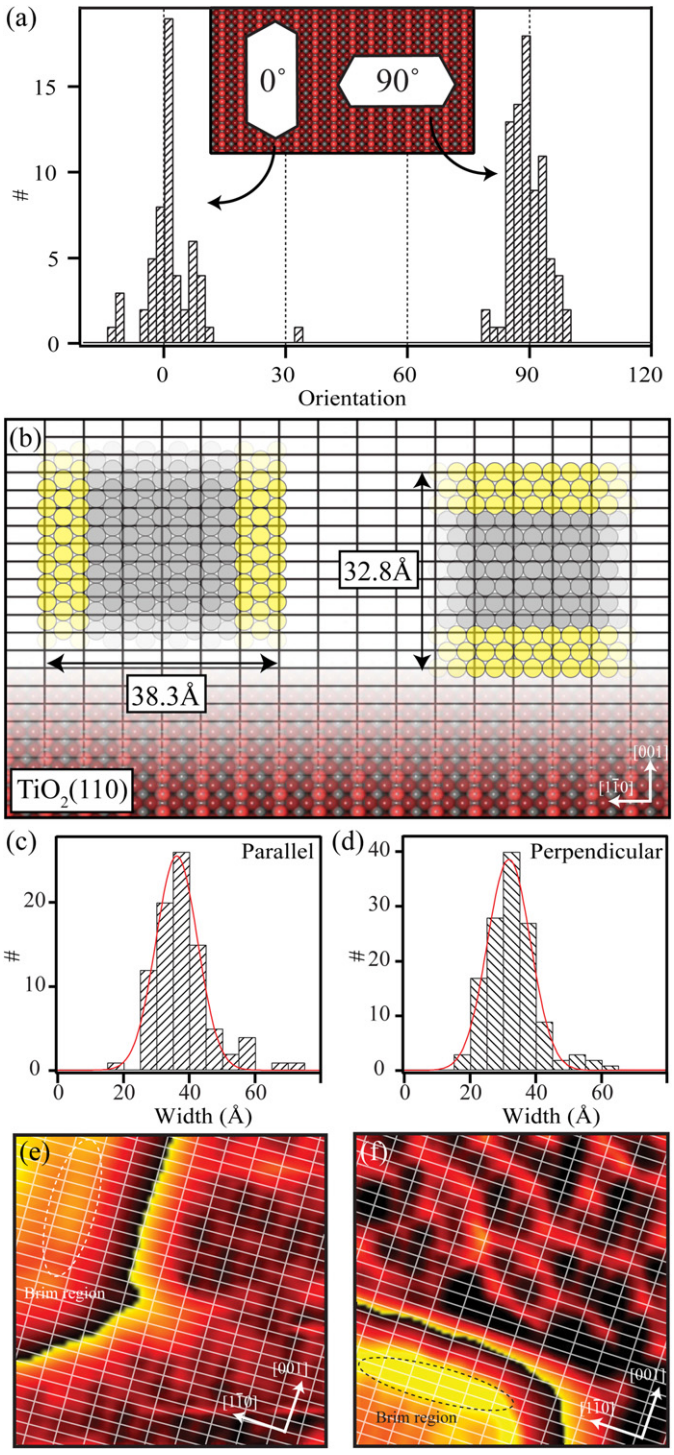

Fig. 5. (a) Rotation distribution of the MoS_2 nanoparticles on the TiO_2 surface with respect to the [001] direction. (b) Two slabs of MoS_2 on a TiO_2(110) surface where the bridging oxygen atoms are represented by the grid. The brim region of the nanoparticles is shown in yellow (color online). (c,d) Width distribution for nanoparticles oriented parallel and perpendicular to the [001] direction, respectively. (e, f) Show two STM images (75 Å × 75 Å) of the edge region of a nanoparticle oriented parallel and a nanoparticle oriented perpendicular to the [001] direction, respectively. The grids show the position of the bridging oxygen atoms.

and we therefore attribute the anisotropic growth observed for the MoS_2 to kinetic limitations in the surface diffusion during particle growth, since strain free islands are only obtained when the particles achieve a width corresponding to multiples of the optimum width (38.3 Å or 32.8 Å).

3.3. Edge structure and support linkages

The atomistic origin of the stronger bonding and favorable orientation associated with the longer edges (γ^*_{Mo} and γ^*_S) of the MoS_2 particles may be associated with the formation of direct chemical Mo–O–Ti or Mo–S–Ti linkages. The resolution of the edge structures in the STM images was limited by the low conductivity of TiO_2 and unfortunately it does not allow a direct atomic-scale analysis of such chemical linkages, but as shown in the high-resolution STM images in Fig. 3d we can still distinguish between the (10$\bar{1}$0) Mo edges and the ($\bar{1}$010) S edges by their appearance. Previous results for Au-supported MoS_2 or multi-layer MoS_2 slabs [12,13] have shown that both edges are imaged with a bright brim extending along the edge of the MoS_2 nanoparticles with the brim of the S edge imaged with a higher intensity. The origin of the brims are distinct electronic edge states pertaining to both the (10$\bar{1}$0) Mo edge and the ($\bar{1}$010) S edge (with H adsorbed) which render the edges metallic as opposed to the otherwise semiconducting MoS_2 slabs, meaning that the edges are imaged bright by the STM due to the enhanced density of electron states. As illustrated in the STM line scan across both edges of the TiO_2 supported particle in Fig. 3e, we can also discriminate between the (10$\bar{1}$0) Mo edge and the ($\bar{1}$010) S edge by the brim height. Both edges seem to be metallic like in the previous studies [12,13], and under the assumption that chemical bonding to the TiO_2 support does not invert the relative brim heights we can therefore assign the brightest edges to ($\bar{1}$010) S edges. However, the width of the brims perpendicularly to the edge is significantly larger for the TiO_2 supported particles, which could indicate that a structural bending of the very flexible MoS_2 plane is present to facilitate direct chemical bonding of the edges. A theoretical treatment may be used to investigate in detail how chemical bonding influences the geometrical and electronic structure of the flat-lying MoS_2 on TiO_2 [21]. Specifically for the MoS_2 on an anatase TiO_2 system, recent density functional theory (DFT) calculations by Arrouvel et al. have already shown how a favorable epitaxial relation between the (101) surface and the Mo-edge of the MoS_2 particles facilitates the formation of multiple Mo–O–Ti and Mo–S–Ti linkages and leads to the formation of edge-up bonded MoS_2 particles [40]. Although a similarly good overlap may be found on the rutile TiO_2(110) surface, as seen in the last section, we observe in the present study no indication of upright standing edge-bonded MoS_2 nanoparticles. However, we expect that the bonding of the MoS_2 nanoparticles in the present study with the (0001) facet oriented parallel with the TiO_2(110) support is also linked to the formation of Mo–O–Ti and Mo–S–Ti linkages at specific positions running along either the [001] or the [1$\bar{1}$0] direction of the TiO_2(110) surface. FTIR [41] and XPS [42] studies of alumina-supported MoS_2 have previously provided evidence of Mo–O–Al linkages and such spectroscopic studies together with DFT calculations of MoS_2 on the rutile TiO_2(110) surface could shed more light on the exact nature of the edge bonding between the MoS_2 nanoparticles and the TiO_2 support.

4. Conclusions and perspective

In conclusion we have used STM to investigate MoS_2 nanoparticles synthesized on a TiO_2(110) support and reveal new insight into an oxide-supported MoS_2-based hydrotreating model catalyst. We show that the TiO_2(110) surface to a great extent controls the growth and accordingly the shape of the MoS_2 nanoparticles, since the orientation and width of the MoS_2 nanoparticles are defined by the well-defined lattice mismatch between the MoS_2 lattice and the TiO_2(110) support. The experimental STM results thus give strong support to recent edge-bonding models from the literature explaining the adhesion of MoS_2 nanoparticles to metal

oxides by chemical linkages at the particle edges. In future experiments it would be interesting to synthesize MoS_2 nanoparticles on another facet of rutile TiO_2 or the anatase polymorph of TiO_2, which will have a different lattice mismatch with respect to the MoS_2 lattice, to investigate whether the width of the synthesized MoS_2 nanoparticles is changed accordingly as expected from the present results. Finally, it would be highly interesting to include both the effect of promoter atoms and the effect of the support. Activity measurements have shown that the HDS activity of thiophene for the same Mo loading is promoted by Co by a factor of 7.6 on alumina, but only by a factor of 3.3 on titania [18]. This finding clearly suggests that the support does not only play a passive role, but there is a synergy between the effects of support and the effects of the promoter atoms. The difference in promotion has recently been proposed to be due to different edge wetting effects for MoS_2 and CoMoS particles on titania and alumina [39], and future STM or Atomic Force Microscopy (AFM) experiments on promoted TiO_2-supported or Al_2O_3-supported MoS_2 nanoparticles may provide detailed information on this interesting synergy effect.

Acknowledgments

The iNANO group gratefully acknowledges financial support from The Danish Research Councils and The Strategic Research Council (NABIIT project “Development of new metal-oxide and -sulphide catalysts”). J.V.L. furthermore acknowledges financial support from Haldor Topsøe A/S, the Carlsberg Foundation and the Lundbeck Foundation. Discussions with K.G. Knudsen and B. Hinnemann are also gratefully acknowledged.

References

[1] H. Topsøe, B.S. Clausen, F.E. Massoth, Hydrotreating Catalysis, Science and Technology, Springer Verlag, Berlin, 1996.
[2] R. Prins, in: G. Ertl, H. Knözinger, F. Schüth, J. Weitkamp (Eds.), Handbook of Heterogeneous Catalysis, Wiley–VCH, Weinheim, 2008, p. 2695.
[3] D.D. Whitehurst, T. Isoda, I. Mochida, Adv. Catal. 42 (1998) 345–471.
[4] K.G. Knudsen, B.H. Cooper, H. Topsøe, Appl. Catal. A 189 (1999) 205–215.
[5] C. Song, Catal. Today 86 (2003) 211–263.
[6] M. Breysse, C. Geantet, P. Afanasiev, J. Blanchard, M. Vrinat, Catal. Today 130 (2008) 3–13.
[7] R. Prins, V.H.J. de Beer, G.A. Somorjai, Catal. Rev.-Sci. Eng. 31 (1989) 1–41.
[8] T.F. Hayden, J.A. Dumesic, J. Catal. 103 (1987) 366–384.
[9] T. Shido, R. Prins, J. Phys. Chem. B 102 (1998) 8426–8435.
[10] P.J. Kooyman, E.J.M. Hensen, A.M. de Jong, J.W. Niemantsverdriet, J.A.R. van Veen, Catal. Lett. 74 (2001) 49–53.
[11] S. Helveg, J.V. Lauritsen, E. Lægsgaard, I. Stensgaard, J.K. Nørskov, B.S. Clausen, H. Topsøe, F. Besenbacher, Phys. Rev. Lett. 84 (2000) 951–954.
[12] J.V. Lauritsen, M.V. Bollinger, E. Lægsgaard, K.W. Jacobsen, J.K. Nørskov, B.S. Clausen, H. Topsøe, F. Besenbacher, J. Catal. 221 (2004) 510–522.
[13] J. Kibsgaard, J.V. Lauritsen, E. Lægsgaard, B.S. Clausen, H. Topsøe, F. Besenbacher, J. Am. Chem. Soc. 128 (2006) 13950–13958.
[14] J.V. Lauritsen, M. Nyberg, R.T. Vang, M.V. Bollinger, B.S. Clausen, H. Topsøe, K.W. Jacobsen, F. Besenbacher, E. Lægsgaard, J.K. Nørskov, F. Besenbacher, Nanotechology 14 (2003) 385–389.
[15] J.V. Lauritsen, S. Helveg, E. Lægsgaard, I. Stensgaard, B.S. Clausen, H. Topsøe, F. Besenbacher, J. Catal. 197 (2001) 1–5.
[16] J.V. Lauritsen, J. Kibsgaard, G.H. Olesen, P.G. Moses, B. Hinnemann, S. Helveg, J.K. Nørskov, B.S. Clausen, H. Topsøe, E. Lægsgaard, F. Besenbacher, J. Catal. 249 (2007) 220–233.
[17] R. Candia, O. Sørensen, J. Villadsen, N.-Y. Topsøe, B.S. Clausen, H. Topsøe, Bull. Soc. Chim. Belg. 93 (1984) 763–773.
[18] J. Ramirez, S. Fuentes, G. Diaz, M. Vrinat, M. Breysse, M. Lacroix, Appl. Catal. 52 (1989) 211–224.
[19] K.C. Pratt, J.V. Sanders, V. Christov, J. Catal. 124 (1990) 416–432.
[20] G.M. Dhar, B.N. Srinivas, M.S. Rana, M. Kumar, S.K. Maity, Catal. Today 86 (2003) 45–60.
[21] B. Hinnemann, J.K. Nørskov, H. Topsøe, J. Phys. Chem. B 109 (2005) 2245–2253.
[22] P. Raybaud, D. Costa, M.C. Valero, C. Arrouvel, M. Digne, P. Sautet, H. Toulhoat, J. Phys. Condens. Matter 20 (2008).
[23] Y.V. Joshi, P. Ghosh, M. Daage, W.N. Delgass, J. Catal. 257 (2008) 71–80.
[24] L. Coulier, J.A.R. van Veen, J.W. Niemantsverdriet, Catal. Lett. 79 (2002) 149–155.
[25] E. Lægsgaard, F. Besenbacher, K. Mortensen, I. Stensgaard, J. Microscopy 152 (1988) 663–669.
[26] U. Diebold, Surf. Sci. Rep. 48 (2003) 53–229.
[27] A.L. Linsebigler, G.Q. Lu, J.T. Yates, Chem. Rev. 95 (1995) 735–758.
[28] M.A. Henderson, Surf. Sci. Rep. 46 (2002) 5–308.
[29] J. Tersoff, D.R. Hamann, Phys. Rev. B 31 (1985) 805–813.
[30] S. Wendt, R. Schaub, J. Matthiesen, E.K. Vestergaard, E. Wahlström, M.D. Rasmussen, P. Thostrup, L.M. Molina, E. Lægsgaard, I. Stensgaard, B. Hammer, F. Besenbacher, Surf. Sci. 598 (2005) 226–245.
[31] S. Wendt, J. Matthiesen, R. Schaub, E.K. Vestergaard, E. Lægsgaard, F. Besenbacher, B. Hammer, Phys. Rev. Lett. 96 (2006).
[32] O. Bikondoa, C.L. Pang, R. Ithnin, C.A. Muryn, H. Onishi, G. Thornton, Nat. Mater. 5 (2006) 189–192.
[33] M.A. Henderson, Surf. Sci. 355 (1996) 151–166.
[34] M.V. Bollinger, J.V. Lauritsen, K.W. Jacobsen, J.K. Nørskov, S. Helveg, F. Besenbacher, Phys. Rev. Lett. 87 (2001) 196803.
[35] M.V. Bollinger, K.W. Jacobsen, J.K. Nørskov, Phys. Rev. B 67 (2003) 085410.
[36] J.V. Lauritsen, M.V. Bollinger, E. Lægsgaard, K.W. Jacobsen, J.K. Nørskov, B.S. Clausen, H. Topsøe, F. Besenbacher, J. Catal. 221 (2004) 510–522.
[37] H. Schweiger, P. Raybaud, G. Kresse, H. Toulhoat, J. Catal. 207 (2002) 76–87.
[38] W.L. Winterbottom, Acta Metall. 15 (1967) 303–310.
[39] D. Costa, C. Arrouvel, M. Breysse, H. Toulhoat, P. Raybaud, J. Catal. 246 (2007) 325–343.
[40] C. Arrouvel, M. Breysse, H. Toulhoat, P. Raybaud, J. Catal. 232 (2005) 161–178.
[41] N.-Y. Topsøe, H. Topsøe, J. Catal. 139 (1993) 631–640.
[42] E.J.M. Hensen, V.H.J. de Beer, J.A.R. van Veen, R.A. van Santen, Catal. Lett. 84 (2002) 59–67.